THE ASTROPHYSICAL JOURNAL, 527:80–85, 1999 December 10

TEMPERATURE MAP OF THE COMA CLUSTER OF GALAXIES

M. WATANABE, K. YAMASHITA, A. FURUZAWA, H. KUNIEDA, AND Y. TAWARA
Department of Physics, Nagoya University, Furo-cho, Chikusa-ku, Nagoya 464-8602, Japan

AND

H. HONDA
Institute of Space and Astronautical Science, 1-1, Yoshinodai, 3-chome, Sagamihara, Kanagawa 229-8510, Japan; honda@astro.isas.ac.jp
Received 1999 February 25; accepted 1999 July 26

ABSTRACT

We present a temperature map of the Coma Cluster of galaxies with an angular resolution of 8′ corresponding to 320 kpc ($H_0 = 50$ km s^{-1} Mpc^{-1}) and an angular extent of 1.°5. The temperature was derived from the hardness ratio of two energy bands, 0.5–3 and 3–10 keV. The X-ray image in the 0.5–10 keV band was also deconvolved from the observed data with the angular resolution of 2′. We have refined the complex response function of the *ASCA* telescope, taking into account the off-axis angle and the energy of incident X-rays in this analysis. The temperature map indicates that a hot region ($kT = 11$–14 keV) is largely extended to the northwest 15′–40′ off from the cluster center, while a cool region ($kT \sim 5$ keV) is 20′ off to the southeast. Another cool region is identified with the subcluster associated with the cD galaxy NGC 4839. These observational features can be interpreted in the context of the subcluster-cluster merging.

Subject headings: galaxies: clusters: individual (Coma) — X-rays: galaxies

1. INTRODUCTION

The Coma Cluster of galaxies had been considered as an archetype of a regular and well-relaxed system because of its symmetric distributions of galaxies and X-ray surface brightness. However, recent optical and X-ray observations reveal the detailed structures of galaxy distribution and X-ray–emitting gas in this cluster. Mellier et al. (1988) identified 1630 member galaxies and found several galaxy groups around bright galaxies including NGC 4889, NGC 4874, NGC 4911, and NGC 4839 within an angular extent of 2.°8 based on the color-magnitude relation for early-type galaxies. The X-ray images were observed by *Einstein* (Jones & Forman 1999), *EXOSAT* (Branduardi-Raymont et al. 1985), and *ROSAT* (Briel, Henry, & Böhringer 1992; White, Briel, & Henry 1993; Vikhlinin, Forman, & Jones 1994, 1997). The *ROSAT* X-ray image clearly shows substructures in the Coma Cluster. Colless & Dunn (1996) and Biviano et al. (1996) measured the radial velocities of member galaxies and constructed magnitude-selected and velocity-selected galaxy-density distributions. They obtained a picture consistent with the *ROSAT* X-ray image.

The emission-weighted gas temperature over the whole cluster was measured to be 8.5 keV by nonimaging observations of *Tenma* (Okumura et al. 1988; Hughes et al. 1988b), *EXOSAT* (Hughes, Gorestein, & Fabricant 1988a), and *Ginga* (Hatsukade 1989). Honda et al. (1996) revealed the large-scale inhomogeneity of the temperature in the range of 5–11 keV with *ASCA* observations. These temperatures were derived from the spectral fitting of *ASCA* data integrated within a circle 30′ in diameter. Donnelly et al. (1999) analyzed the central core ($r \leq 18'$) of the Coma Cluster with an angular resolution of 5′ and found hot and cool regions. A hot region was found with a temperature of around 13 keV displaced north from the central peak of emission. A cool spot was found with a temperature of 4–6 keV and associated with a filament of X-ray emission extending southeast from the cluster center detected by *ROSAT* (Vikhlinin et al. 1997).

Recent simulations of cluster merging show that just after the merger, the cluster has a relatively symmetric X-ray surface brightness distribution but a nonisotropic plasma temperature distribution (Roettiger, Loken, & Burns 1997; Roettiger, Stone, & Mushotsky 1998; Schindler & Muller 1993). So it is important to examine the plasma temperature distribution of a cluster in order to know whether it is well relaxed or not. It is well known that many clusters that have nearly symmetric surface brightness distribution show isothermal or symmetric temperature distribution. However, some clusters apparently show asymmetric temperature distribution, as was reported for A2256 (Markevitch & Vikhlinin 1997); A754 (Henriksen & Markevitch 1996); A2319 (Markevitch 1996); A85, A2657, and A3391 out of 30 nearby clusters (Markevitch et al. 1998); and Cygnus A, A3667, and A2065 (Markevitch, Sarazin, & Vikhlinin 1999).

In this paper, we report on the temperature map with the angular resolution of 8′ and deconvolved image in the 0.5–10 keV band with 2′ in the angular extent of 1.°5, using spectroimaging data of *ASCA*. We have carefully examined the response function of *ASCA* telescope calibrator observations of the point source of 3C 273, as is described along with the analysis method in § 2. The observational results are presented in § 3 and discussed with simulations of subcluster-cluster merging in § 4.

2. ANALYSIS METHOD

The X-ray–emitting region of the Coma Cluster was fully covered with 14 different pointings of the *ASCA* gas-imaging spectrometer (GIS), as described in Honda et al. (1996). The 28 X-ray images taken in the 0.5–10 keV band with two GIS detectors (GIS2 and GIS3) were screened with *ASCA* standard processing tools (Arnaud 1993), with the criteria of minimum Earth elevation angle of 5° and a cutoff rigidity of less than 6 GeV c^{-1}. They are combined together and shown in Figure 1 after the correction of exposure time and boresight and the subtraction of background.

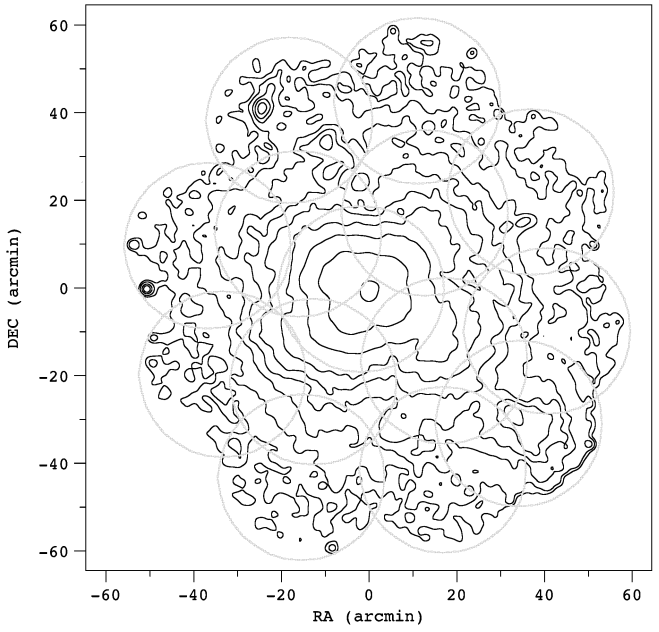

FIG. 1.—Fourteen pointed *ASCA* observations are shown with a circle of radius 18′ (GIS field of view) superposed on a contour map of the observation after corrections for exposure time and background subtraction. The image center is R.A. = 194°.9278, decl. = 27°.9707 (J2000).

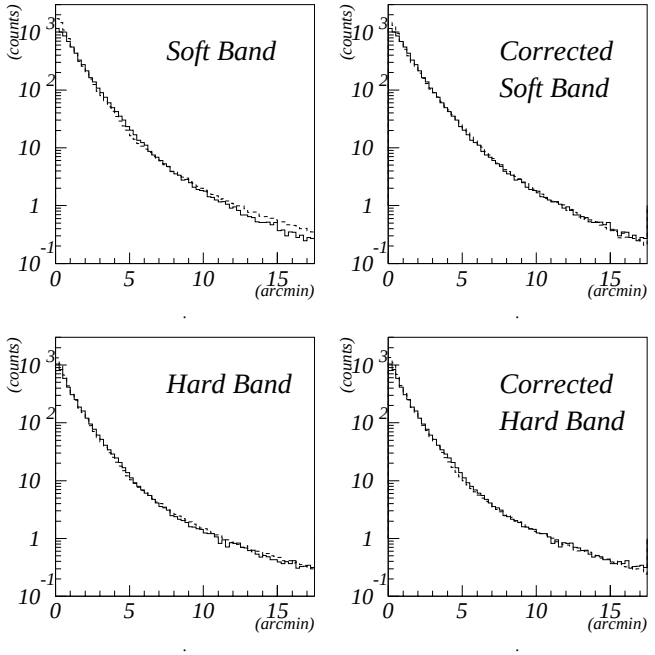

FIG. 2.—Radially averaged PSF of 3C 273 (*solid line*) and simulation (*dashed line*) for soft (0.5–3.0 keV) and hard (3.0–10.0 keV) bands. The left and right panels are the results before and after tuning the ray-tracing program, respectively.

For the spectroimaging analysis, we construct three kinds of X-ray images, dividing the energy region into 0.5–3 keV (soft band), 3–10 keV (hard band), and 0.5–10 keV (total band). The total-band image is binned into a pixel of 2′ × 2′, taking into account the angular response of the *ASCA* X-ray telescope (XRT) with 2′.9 in half-power diameter. The pixel size of the soft- and hard-band images is increased to 8′ × 8′ for deriving the hardness ratio (HR) with good statistics. We exclude pixels whose numbers of counts are less than 20 for the total band and less than 200 for the soft and hard bands from the image analysis. The HR map was made from the intensity ratio of the hard-band image to the soft-band image. In order to proceed with the image deconvolution, we have to know the precise response function of XRT.

The *ASCA* complex image caused by the response function of the XRT made of the multinested thin-foil mirrors can be reproduced well by the ray-tracing program. This program was originally prepared by Tsusaka et al. (1995) and modified by Kunieda et al. (1995). We compare the simulated point-spread function (PSF) of a point source with four observed radial distributions of 3C 273 at different off-axis angles. These positions are 4′.8, 8′.0, 5′.8, and 6′.9 off from the XRT optical axis for GIS2 and 8′.4, 5′.8, 9′.6, and 2′.3 for GIS3. One of the results is shown in the left side of Figure 2 divided into the soft and hard bands. The solid line and dashed line represent the observed data and the simulated value, respectively. The fitting is not good enough in the large-angle region, so we further refined this simulation program to fit the 3C 273 data well for both bands, as shown in the right side of Figure 2. This is important in order to correct split-over counts pixel by pixel for extended sources.

This ray-tracing program is incorporated into the *ASCA* full-simulation program. We start simulating X-ray images of the Coma Cluster in the soft, hard, and total bands with initial conditions of a temperature that is 8.5 keV isothermal and a β-model of core radius $R_c = 105$ and $\beta = 0.75$ derived from the *ROSAT* observation (Briel et al. 1992). The total-band image is divided into pixels of 2′ × 2′—the same size as the pixels of the observed data—while the soft- and hard-band images are binned into 8′ × 8′ pixels. HR values are converted to plasma temperatures on the assumption of a Raymond-Smith model with the abundance of 0.2 solar. A simulated HR map and total-band image are iteratively reconstructed by comparing with observed ones. The deconvolution process is carried out in such a way of iterating this simulation until the difference between the data and simulated values is smaller than systematic and statistical errors, as described below. We also confirm that χ^2 reaches the minimum after the iterations.

In the case of the image processing, the total number of counts simulated by the initial condition and response function of the XRT is normalized to the observed counts accumulated over the cluster. Then, we can express the corrected photon number $N_{\rm cor}$ for the ith image pixel as follows:

$$(N_{\rm cor})_i = \frac{(N_{\rm obs})_i}{(N_{\rm sim})_i}\,(N_{\rm src})_i\,, \quad \sum_i (N_{\rm obs})_i = \sum_i (N_{\rm sim})_i\,, \qquad (1)$$

where $(N_{\rm src})_i$ is the initial photon number, $(N_{\rm obs})_i$ is the observed counts, and $(N_{\rm sim})_i$ are simulated values given as $(N_{\rm src})_i$ folded with the XRT response function. We take this corrected image as the source image for the next simulation. When $(N_{\rm obs})_i/(N_{\rm sim})_i$ is close to unity within the error, the iteration is terminated.

In the case of the HR map, we begin with calculating the difference between the observed HR ($\rm HR_{obs}$) and the simulated one ($\rm HR_{sim}$) for the ith pixel:

$$\Delta(\rm HR)_i = (HR_{obs})_i - (HR_{sim})_i\,, \qquad (2)$$

where $(\rm HR_{sim})_i$ is in unit pixels of 8′ × 8′, calculated with the initial conditions of isothermal temperature and β-model.

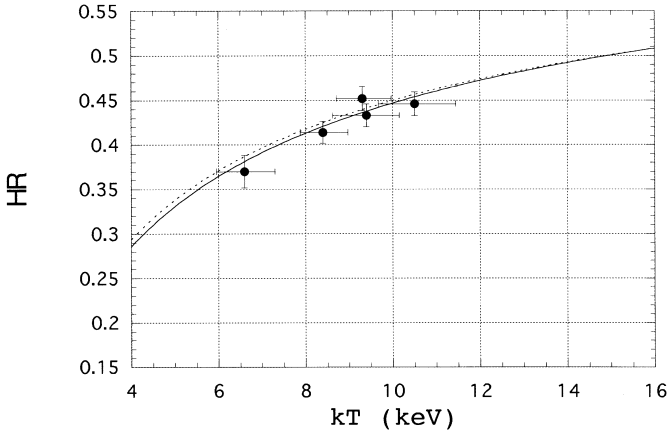

FIG. 3.—HR vs. kT calculated by eqs. (3) (*solid line*) and (4) (*dotted line*). Values of $(HR_{obs})_i$ are plotted with solid circles against kT derived from the spectral fitting in the central region. Error bars are 90% confidence level.

Then we have to derive the relation between $\Delta(HR)_i$ and $\Delta(kT)_i$ from the *ASCA* simulation. The relation of HR to kT is expressed in equations (3) and (4) for off-axis angles of 5′ and 15′, respectively, and shown in Figure 3:

$$HR = -0.9027kT^{-0.4189} + 0.7908 , \quad (3)$$

$$HR = -0.8607kT^{-0.4526} + 0.7534 . \quad (4)$$

HRs slightly depend on the off-axis angle, which corresponds to a difference in kT of a few tenths keV. This is not significant within the statistical errors of $\Delta(HR)_i$. In order to verify this analysis method, we derive kT from the spectral fitting of the Raymond-Smith model to observed spectra in pixels of the central region where the contribution of spurious counts split over from adjacent pixels is insignificant. These values of $(HR_{obs})_i$ against kT are also plotted with error bars in Figure 3 and are confirmed to be consistent with the HR-kT relation obtained by equations (3) and (4).

Consequently, we can convert $\Delta(HR)_i$ to $\Delta(kT)_i$ by differentiating equations (3) and (4) by kT. Then the corrected temperature is obtained as follows:

$$(kT_{cor})_i = (kT_{src})_i + \Delta(kT)_i , \quad (5)$$

where $(kT_{src})_i$ is an initial temperature given as 8.5 keV for the first simulation. This corrected temperature in each pixel is used as the source temperature for the next simulation.

Finally, each pixel of the total-band image $(N_{cor})_i$ and temperature map $(kT_{cor})_i$ is subdivided into 0.25 and smoothed with a two-dimensional Gaussian function with a $\sigma_x = \sigma_y = 1'$ and 4′, respectively.

The statistical errors of temperature are defined as the 1 σ error of HR. While the systematic errors are caused mainly by the uncertainty of the response function of XRT, we regard the difference of kT derived by the before-and-after tuned simulation as the systematic errors. Average systematic errors become smaller than the statistical errors. Typical errors for temperature are estimated to be 1–2 keV near the cluster center, 2–3 keV in the outer cool region, and 3–4 keV in the outer hot region.

3. RESULTS

The temperature map thus obtained is shown in Figure 4 superposed on the total-band image deconvolved from the observed image shown in Figure 1. The position center is R.A. = 194.911 and decl. = 27.945 in J2000. It is noticeable that the extended hot region is located at the northwest, 15′–40′ off from the center, having an extension of about 50′ × 20′ and an arclike structure as shown with red. The temperatures were obtained to be from 11 ± 2 to 14 ± 3 keV, exhibiting the strong contrast with other regions. The existence of this hot region has been pointed out by Honda et al. (1996). This fact is firm evidence that this cluster is not dynamically well relaxed, since a relaxed cluster can never have such a hot and extended region in the outer envelope. The small hot region located 5′ from the center to the north as reported by Donnelly et al. (1999) is confirmed with $kT = 12 \pm 2$ keV. We can also see the small hot regions 40′ southeast of the cluster center and between the NGC 4839 subcluster and the main cluster. Lower limits for these two regions were derived to be 12.9 and 13.6 keV, respectively, which were obviously higher temperatures than the 8.5 keV mean cluster temperature.

The extended cool region ($kT \sim 5 \pm 1$ keV) is located to the southeast, ∼20′ from the center, with a size of about 20′ × 10′. Part of this cool region was reported by Donnelly et al. (1999), coinciding with a 4.5–6 σ excess in the intensity discovered by wavelet analysis of *ROSAT* images (Vikhlinin et al. 1997). This image excess around NGC 4911 is also found to be ∼6 σ in the 0.5–10 keV band, as shown in Figure 5. This figure represents the image excess above a radially symmetric β-model of $R_c = 9.3$ and $\beta = 0.66$ derived from the radial profile of the total-band image. These values are slightly smaller than those of *ROSAT* (Briel et al. 1992), though the energy band is different. We use all the data, while Briel et al. (1992) exclude the pie-shaped wedge from position angle 200° to 260° centered on the main cluster in order to avoid the NGC 4839 group. The overall image shows more extension toward the west side rather than toward the east compared with a radially symmetric β-model. The small hot spot 40′ to the southeast from the center does not coincide with any image excess in Figure 5.

Another cool region ($kT = 5 \pm 3$ keV) associated with the subcluster around cD galaxy NGC 4839 corresponds to a 6 σ image excess, relative to the surface brightness distribution of the β-model. We find an 8 σ image excess extending 10′ to the north, gradually decreasing to 3 σ between the cluster center and the subcluster.

4. DISCUSSION

Our observational results confirm that the Coma Cluster is not a dynamically well-relaxed system, but an ongoing merger, as first revealed morphologically by *ROSAT* observations (Briel et al. 1992; White et al. 1993). We have obtained the 0.5–10 keV X-ray image and a temperature map over the whole cluster. These spectroimaging data include most of the information except for the abundance extracted from previous observations, which allows us better understanding of the dynamical structure of the cluster for comparison with optical observations.

The large, extended hot region to the northwest shown in Figure 4 shows no clear correlation to enhancements in the X-ray image in Figure 5. This fact suggests that cluster merging could shock-heat the intracluster gas and result in hot regions. Simulations of cluster-subcluster merging were extensively studied by Schindler & Muller (1993) and Roettiger et al. (1997, 1998). They show spatial distributions of

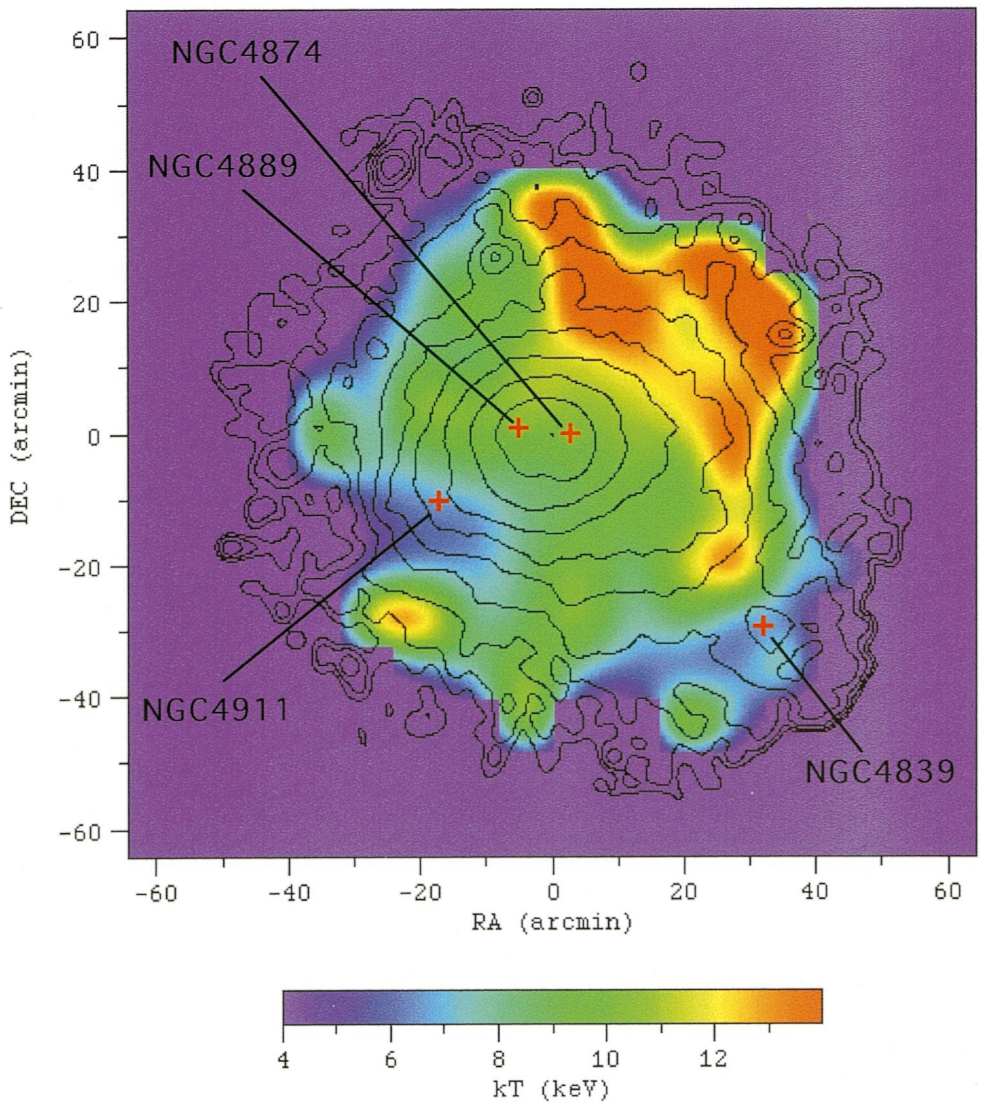

FIG. 4.—Color-coded temperature map superposed on the contour map of the total band. The positions of four bright galaxies are indicated with crosses. Contour levels are 0.3%, 0.6%, 1.1%, 2.1%, 4.0%, 7.7%, 14.6%, 27.7%, 52.6%, and 100% of the peak.

X-ray surface brightness and temperature as functions of the mass ratio, velocity, separation, epoch, and viewing direction from the merging axis. According to Roettiger et al. (1998), the hot region would be formed in the outer region ~ 1 Gyr after the epoch of merging. On the other hand, Biviano et al. (1996) find that the main body of the Coma Cluster would be formed by fainter galaxies and that galaxy groups surrounding the brightest galaxies have been infalling onto the main body, based on the intensive analysis of optical data of the density, color magnitude, and radial velocities of merger galaxies. They suggest that the infall of the group associated with NGC 4874 may have induced the pressure wave in the X-ray–emitting gas. In this context we interpret the formation of the northwest hot region as evidence that the galaxy group around NGC 4874 has merged onto the main body from the southeast and creates the shock-heated region in the northwest.

The cool region 20′ to the southeast from the center overlaps the image excess in Figure 5 and extends more to the south from a trail found by Vikhlinin et al. (1997). It seems to be a subcluster left behind by an infalling galaxy group around NGC 4911. Probably a small hot spot 40′ off to the southeast from the center could be associated with the infall of this galaxy group.

Another cool region 40′ to the southwest from the center corresponds to the subcluster around NGC 4839, as was clearly observed by *ROSAT* (Briel et al. 1992; White et al. 1993). Colless & Dunn (1996) and Biviano et al. (1996) found evidence of an interaction of this subcluster with the main body from their analysis of galaxy counts and radial velocity distribution. The mass of the subcluster is estimated to be one-tenth of the cluster mass (Colless & Dunn 1996). In this context there remains a hot region between the cluster center and the subcluster displaced from the merging axis, which corresponds to the hot region in Figure 4 and the enhancement in Figure 5. This region would be formed by the shock-heating in the cluster-subcluster merging. Simulations of a premerger also support this configuration.

5. CONCLUSION

We have deduced the dynamical structure of the Coma Cluster from the temperature map and image excess obtained by *ASCA*, incorporating the results of optical

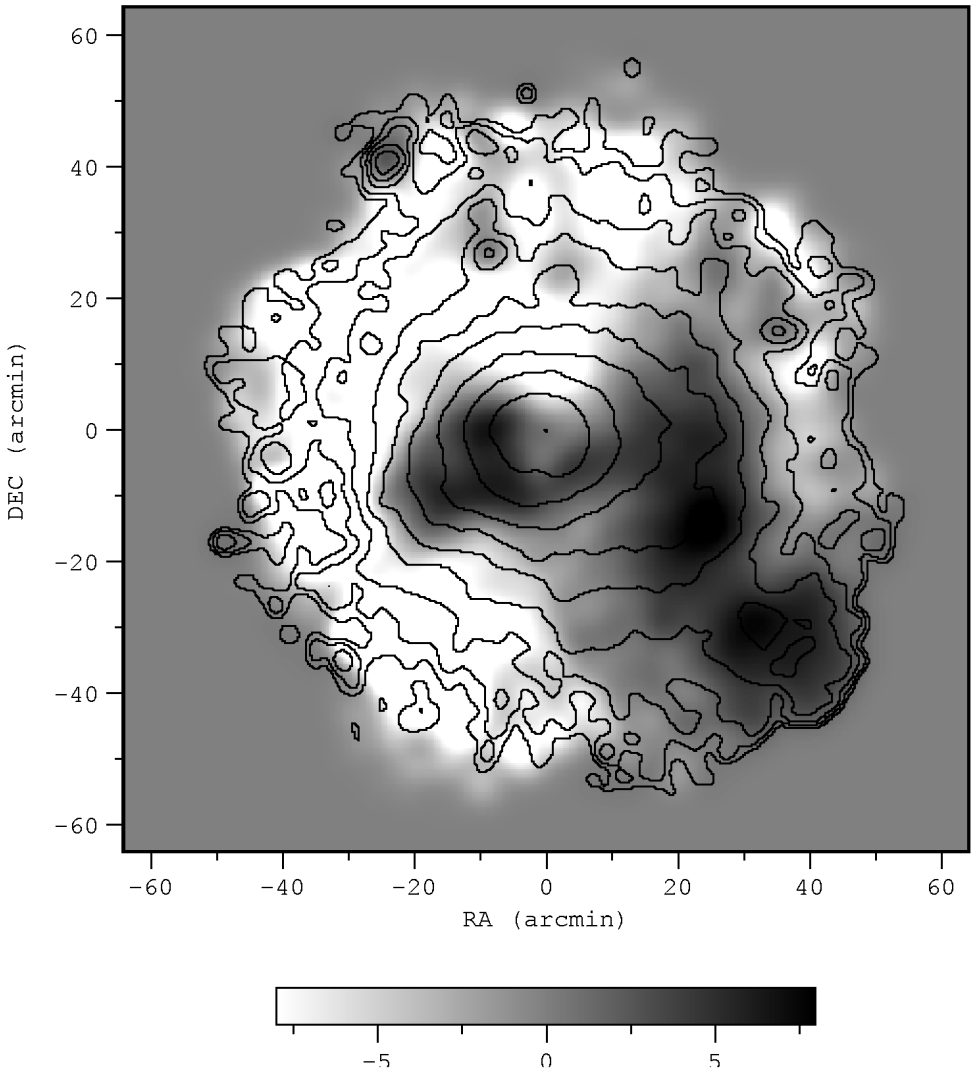

FIG. 5.—Image excess deviated from a β-model ($R_c = 9'.3$, $\beta = 0.66$) is shown by the gray scale in σ on the contour map of the total band

observations of member galaxies and simulations of cluster merging. Our results confirm and extend previous suggestions and are as follows:

1. The largely extended hot region in the northwest would be formed by the shock-heating induced by the infall of the galaxy group around NGC 4874 to the main body of the Coma from the southeast direction.

2. The cool region in the southeast would be caused by an infalling galaxy group around NGC 4911. This gas is most likely deposited in the wake of the merging group.

3. The subcluster around NGC 4839 is interacting with the main body and has formed a hot region in between.

We thank the XRT, ASCA_ANL, and SimASCA teams for building the analysis system for extended sources. This work was supported in part by a Grant-in-Aid for Scientific Research on Specially Promoted Research, contract 07102007, from the Ministry of Education, Science, Sports, and Culture, Japan. The authors acknowledge the referee for his advice for improving the manuscript.

REFERENCES

Arnaud, K. 1993, *ASCA* Newsl., No. 1
Biviano, A., Durret, F., Gerbal, D., Le Fèvre, O., Lobo, C., Mazure, A., & Slezak, E. 1996, A&A, 311, 95
Branduardi-Raymont, G., Mason, K. O., Murdin, P. G., & Martin, C. 1985, MNRAS, 216, 1043
Briel, U. G., Henry, J. P., & Böhringer, H. 1992, A&A, 259, L31
Colless, M., & Dunn, A. 1996, ApJ, 458, 435
Donnelly, R. H., Markevitch, M., Forman, W., Jones, C., Churazov, E., & Gilfanov, M. 1999, ApJ, 513, 690
Hatsukade, I. 1989, Ph.D. thesis, Osaka Univ.
Henriksen, M., & Markevitch, M. 1996, ApJ, 466, L79
Honda, H., et al. 1996, ApJ, 473, L71
Hughes, J. P., Gorestein, P., & Fabricant, D. 1988a, ApJ, 329, 82
Hughes, J. P., Yamashita, K., Okumura, Y., Tsunemi, H., & Matsuoka, M. 1988b, ApJ, 327, 615
Jones, C., & Forman, W. 1999, ApJ, 511, 65
Kunieda, H., Furuzawa, A., Watanabe, M., & XRT Team. 1995, *ASCA* Newsl., No. 3, 3
Markevitch, M. 1996, ApJ, 465, L1
Markevitch, M., Forman, W. R., Sarazin, C. L., & Vikhlinin, A. 1998, ApJ, 503, 77
Markevitch, M., Sarazin, C. L., & Vikhlinin, A. 1999, ApJ, 521, 526
Markevitch, M., & Vikhlinin, A. 1997, ApJ, 474, 84
Mellier, Y., Mathez, G., Mazure, A., Chauvineau, B., & Proust, D. 1988, A&A, 199, 67
Okumura, Y., Tsunemi, H., Yamashita, K., Matsuoka, M., Koyama, K., Hayakawa, H., Masai, K., & Hughes, J. P. 1988, PASJ, 40, 639
Roettiger, K., Loken, C., & Burns, J. 1997, ApJS, 109, 307
Roettiger, K., Stone, J., & Mushotzky, R. 1998, ApJ, 493, 62
Schindler, S., & Muller, E. 1993, A&A, 272, 137
Tsusaka, Y., et al. 1995, Appl. Opt., 34, 22
Vikhlinin, A., Forman, W., & Jones, C. 1994, ApJ, 435, 162
———. 1997, ApJ, 474, 7
White, S., Briel, J., & Henry, J. 1993, MNRAS, 261, L8